Biochimica et Biophysica Acta 1828 (2013) 455–460

Contents lists available at SciVerse ScienceDirect

Biochimica et Biophysica Acta

journal homepage: www.elsevier.com/locate/bbamem

Biophysical characterization of a binding site for TLQP-21, a naturally occurring peptide which induces resistance to obesity

V. Cassina [a,*], A. Torsello [a], A. Tempestini [a], D. Salerno [a], D. Brogioli [a], L. Tamiazzo [a], E. Bresciani [a], J. Martinez [b], J.A. Fehrentz [b], P. Verdié [b], R.J. Omeljaniuk [c], R. Possenti [d], L. Rizzi [a], V. Locatelli [a], F. Mantegazza [a]

[a] Department of Experimental Medicine, University of Milano-Bicocca, Via Cadore 48, 20900, Monza (MB) Italy
[b] Institut de Biomolécules Max Mousseron, UMR 5247, CNRS, Universités Montpellier 1, Montpellier 2, 34093, Montpellier, France
[c] Department of Biology, Lakehead University, 955 Oliver Road, Thunder Bay, ON, Canada P7B 5E1
[d] Dept Medicine of Systems, University of Rome Tor Vergata, Viale Montpellier 1, and CNR-IFT, 00133, Rome, Italy

ARTICLE INFO

Article history:
Received 10 May 2012
Received in revised form 19 October 2012
Accepted 22 October 2012
Available online 30 October 2012

Keywords:
TLQP-21
VGF
Ligand–receptor
Atomic force Microscopy (AFM)
CHO
Fluorescence

ABSTRACT

Recently, we demonstrated that TLQP-21 triggers lipolysis and induces resistance to obesity by reducing fat accumulation [1]. TLQP-21 is a 21 amino acid peptide cleavage product of the neuroprotein VGF and was first identified in rat brain. Although TLQP-21 biological activity and its molecular signaling is under active investigation, a receptor for TLQP-21 has not yet been characterized. We now demonstrate that TLQP-21 stimulates intracellular calcium mobilization in CHO cells. Furthermore, using Atomic Force Microscopy (AFM), we also provide evidence of TLQP-21 binding-site characteristics in CHO cells. AFM was used in force mapping mode equipped with a cantilever suitably functionalized with TLQP-21. Attraction of this functionalized probe to the cell surface was specific and consistent with the biological activity of TLQP-21; by contrast, there was no attraction of a probe functionalized with biologically inactive analogues. We detected interaction of the peptide with the binding-site by scanning the cell surface with the cantilever tip. The attractive force between TLQP-21 and its binding site was measured, statistically analyzed and quantified at approximately 40 pN on average, indicating a single class of binding sites. Furthermore we observed that the distribution of these binding sites on the surface was relatively uniform.

1. Introduction

A fundamental problem in biophysical research is the study of the physical interaction between of a ligand and its receptor. The recent development of techniques which analyze biological systems at the nano-scale allows quantification of ligand–receptor binding forces. Indeed, binding strength is a significant parameter for understanding the characteristics of interaction and it is not easily investigated by standard biochemical measurements. Recently, several studies were focused on TLQP-21, a peptide that induces anorexic effects, activates lipolysis and blunts obesity induced by diet [1]. Given the increasing spread of obesity in industrialized countries, TLQP-21 and its biological effects are receiving great attention. However, the receptor(s) which mediate TLQP-21 effects has (have) not been characterized, and there is little information on TLQP-21 mechanisms of action.

TLQP-21 is a derivative of the better known VGF, a protein expressed in the central and peripheral nervous systems [2]. In the adult rat brain VGF is expressed in several areas (hippocampus, hypothalamus, pituitary gland, olfactory system, cerebral cortex), and in many cerebral nuclei (thalamic, septal, amygdaloid, brain stem) [3]. These areas are involved in the regulation of feeding, reproduction, stress responsiveness, and general homeostasis [4,5]. The VGF aminoacidic sequence shows many cleavage recognition sites and is processed by the pro-hormone convertases PC1/3 and PC2 stored in secretory granules to yield several peptides [6,7]. TLQP-21 (VGF $^{556-576}$) was immunopurified for the first time from rat brain [1] and subsequently localized in gastric tissue [8], adrenal medulla [9] and adrenergic neurons [10] by immunohistochemical techniques.

Since knockout mice for VGF are smaller and thinner compared to their wild type [11], it was expected that the products of the VGF protein processing should have an opposite effect on fat deposition. Surprisingly, prolonged administration of TLQP-21 increased energy expenditure and decreased fat deposition in the adipose tissue (brown and white), preventing increases in weight [1]. Moreover, TLQP-21 caused a decrease of weight and reduced intra-abdominal white fat deposits in Siberian hamsters [12] and inhibited inflammatory pain modulation [13]. It was also demonstrated that TLQP-21, by acting on gastric tissue [6], could have a role in the control of gastrointestinal motility and metabolic functions [14], as well as in regulation of gastric acid secretion [15].

In recent years, efforts have been made to characterize the effects of TLQP-21; however, little is known about the pathways and molecular

* Corresponding author.
E-mail address: valeria.cassina@unimib.it (V. Cassina).

0005-2736/$ – see front matter © 2012 Elsevier B.V. All rights reserved.
http://dx.doi.org/10.1016/j.bbamem.2012.10.023

targets of this peptide. It was recently demonstrated that adipocyte membranes express a high affinity binding site for TLQP-21 and that the peptide stimulates a pro-lipolytic effect [16], but the receptor for TLQP-21 is still unknown.

Atomic Force Microscopy (AFM) represents a powerful tool in biophysical research and it is widely used for both imaging of biological sample with nanometric resolution [17,18] or force spectroscopy studies. In these experiments we used the AFM at nm order of imaging resolution and pN force sensitivity. By performing force measurement, here we show the presence and the plasma membrane topological distribution of a TQLP-21 binding site on the Chinese Hamster Ovary (CHO) cell line. AFM measures the interaction force between a microscopic cantilever with a sample's surface [19]. In this study, we used AFM in force mapping mode [20–22] with a cantilever functionalized with TLQP-21. We measured ligand-binding site interaction forces using the functionalized cantilever as a scanning probe over the cell surface. This approach allowed us to quantitate the interaction forces between ligand and binding site and to map the topological distribution of the binding sites on the cell surface [23–25].

2. Materials and methods

2.1. Chemicals

TLQP-21 (TLQPPASSRRRHFHHALPPAR), LRP-21 (LRPSHTRPAHQSF ARPLHRPA), and biotin-TLQP-21 (Biotin-TLQPPASSRRRHFHHALPPAR) were synthesized by conventional solid phase synthesis. Biotin-TLQP-21 was synthesized to functionalize the streptavidinated AFM cantilever tips. LRP-21 is a scrambled version of the TLQP-21 peptide, and was used to distinguish selectivity of the binding site for TLQP-21. Unless otherwise specified, all other reagents were from Sigma-Aldrich (St Louis, MO).

2.2. Cell culture

Embryonic mouse hypothalamic cell lines N38, N41 and N42, and CHO and rat GH3 cell lines were screened for their ability to respond to TLQP-21 stimulation. Cells were plated at 20,000 cells/well in black walled, clear bottom 96-well plates (Corning, Germany) and cultured for two days up to 80–90% confluence.

2.3. Intracellular Ca^{2+} mobilization assay

TLQP-21 biological activity was assessed on the basis of changes in intracellular free calcium revealed by fluorescence assay. Cells were preloaded with a fluorescent agent, then exposed to TLQP-21. In comparable systems, ligand–receptor interaction may induce a release (mobilization) of calcium from intracellular stores. Free calcium then interacts with the fluorescent agent to trigger a degree of light emission proportional to the calcium available. Fluorescence signals were normalized relative to basal values (total fluorescence divided by basal fluorescence) measured before peptide injection and signals were expressed as a percentage of increment.

Cells were incubated in darkness with 100 μl HBSS containing HEPES 20 mM, probenecid 2.5 mM, and the fluorescent agent FLUO-4 NW 4.5 μ M (Molecular Probes, Eugene, OR, USA) at 37 °C and 5% CO_2 for 45 min. Fluorescence emissions were measured with the multi-label spectrophotometer VICTOR3 (Perkin Elmer) at 485/535 nm (excitation/emission filters) every second for the 20 s preceding and for the 60 s following peptide exposure. TLQP-21 (10^{-9} to 10^{-5}M), LRP-21 (10^{-5} M) and biotin-TLQP-21 (10^{-5} M) were dissolved in HBSS and injected into the wells by an automated injector system. Data shown are the mean of measurements obtained in 6 different wells for each treatment.

2.4. Force measurements, AFM tips functionalization and data analysis

AFM force measurements on living cells were performed with a Nanowizard II (JPK instruments, Berlin), with the overlay option, which allowed a direct view of the sample and the cantilever on the same image (see Fig. 1). In this set up, the AFM head is placed on a Zeiss optical microscope and data acquisition is performed using JPKs software.

Silicon nitride (Si_3N_4) AFM probes (spring constant 0.06 N/m, tip radius ~ 10 nm) with streptavidin coating (CT.AU.SN, Novascan Technologies, Inc., Ames, USA) were incubated in a solution of 4 mM biotin–TLQP-21 for 1.5 h at room temperature. In this way peptide was bound to the tip via streptavidin–biotin interaction. After rinsing thoroughly with PBS, the functionalized probe was immediately used without drying.

In AFM force-mapping mode measurements, the probe, moving in *z*-direction, was brought alternately into and out of contact with the sample surface. During each approach and retraction cycle, the cantilever deflections versus the separation between the tip and the surface were recorded and plotted as approach and retraction curves. A non-interaction zone corresponded to a situation where the tip was far away from the surface and there was no cantilever deflection. In principle, by moving the probe toward the cells, the tip comes in contact with surface. This induces a cantilever deflection; the shape of this portion of the curve depends on the stiffness of the sample and it is expected to be linear only if there is no sample deformation. By moving the tip upwards, the cantilever undergoes an hysteresis in the adhesion zone until the tip detaches from the surface (pull-off) (see insets of Fig. 5a and Fig. 5b). The deflection measured at the pull-off (depth of the minimum of the curve) is proportional to the force of adhesion established with the binding site. Finally, the adhesion was statistically analyzed by collecting several approach and retraction cycles and reporting the depths of the pull-off in a histogram (see Fig. 5). The overall soundness of the procedure of functionalizing the cantilever by streptavidin–biotin binding is established by other classical works reported in literature [26–29] confirming the fact that the streptavidin–biotin binding (in the order of more than 150 pN) is much stronger than the ligand–receptor interaction under investigation [23,30–32].

By using functionalized tips against the living cells' membrane, it was possible to study specific ligand-binding site interactions. Force measurements between the TLQP-21 functionalized tip and the cell surface were performed in HBSS with 20 mM HEPES at 30 °C in force-mapping mode. Several sets of 1600 force curves over an area

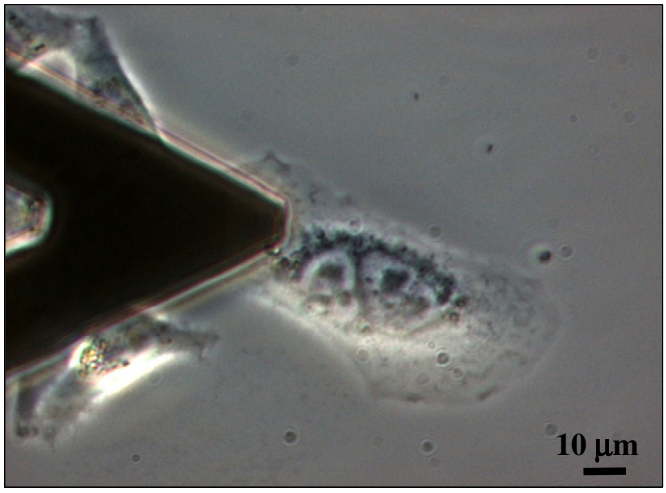

Fig. 1. Phase contrast image of an AFM cantilever placed above a CHO cell. Image acquired thanks to the direct overlay of the AFM and the optical microscope. The dark triangle is the AFM cantilever.

of $2\times2\ \mu m^2$ were acquired on different points over the cell surface using 2 μm *z*-range, 2 μm/s *z* scan rate and a trigger on the deflection in order to control the maximum force. Control experiments were performed on CHO cells with non functionalized tips and an N38 cell line (non-biologically responsive to TLQP-21) using both similarly functionalized and non-functionalized tips (Fig. 5b and Fig. 6c–e). To preserve the native properties of the cells, in all AFM experiments the cells are maintained alive on a glass cover-slip and measurements were performed in oxygenated HBSS at 30 °C.

The force curve arrays were analyzed off-line with a semiautomatic Matlab routine. The deflection versus distance curves were converted to force distance curves by the relation $F = k \cdot d$ where k is the cantilever spring constant and d is the deflection. The nominal spring constant of each cantilever was verified by the thermal noise calibration method. The typical values of the spring constant were 0.01–0.08 N/m. In order to keep a zero force in the no-interaction zone, a linear contribution was subtracted from each curve. After calculating the root mean square (rms) of the signal in the non-interaction zone, the depth of the adhesion peak (see inset of Fig. 5a) of each force curve was extracted. The sensitivity of our measurements can be estimated as 3 pN by taking in account the noise that characterized the force curves in the non-interaction region where the cantilever is free to oscillate. The amplitude of the measured minima varied from a minimum of 3 pN, to a maximum of approximately 150 pN. Uncertainties of the mean unbinding force were calculated by the standard error of the mean of the distribution [33,34].

3. Results and discussion

3.1. Intracellular calcium measurements

In preliminary experiments several cell lines (CHO, N38, GH3, N41, N42) were screened for their ability to respond to TLQP-21. Treatment with 10^{-6} M TLQP-21 induced a peak of fluorescence in CHO (see Fig. 2, black dots), whereas N38 (see Fig. 2, black squares), GH3, N41, and N42 (data not shown) were unaffected. Consequently, CHO cells were chosen for further detection and characterization of TLQP-21 binding sites; conversely, the N38 cell line were chosen as a negative control.

TQLP-21 stimulated fluorescence in CHO cells increased with time, reaching maximal levels within 10 s of stimulation and returning to basal levels in about 60 s (see dots in Fig. 2). Qualitatively, this variation of fluorescence as a function of time can be interpreted as the result of two concurrent physical phenomena: the fluorescence switch on (due to the calcium mobilization) and its consequent decay. The mathematics of this toy model is described by the following simple system of differential equations:

$$\begin{cases} \dfrac{dA(t)}{dt} = -\dfrac{A(t)}{\tau_A} \\ \dfrac{dB(t)}{dt} = -\dfrac{B(t)}{\tau_B} + \dfrac{A(t)}{\tau_A} \end{cases} \quad (1)$$

where $A(t)$ represents the population of molecules not yet activated to emit fluorescence, while $B(t)$ is the population of actively fluorescent molecules not yet faded at a given time t. τ_A and τ_B are the characteristic times of the switch on and off the decay of the fluorescence. The measured fluorescence signal is proportional to $B(t)$. Solving the above systems of equations and assuming the initial conditions $A[t=0]=A_0$, $B[t=0]=0$, results:

$$B(t) = \frac{A_0\tau_B}{\tau_A-\tau_B}\left(e^{-\frac{t}{\tau_A}} - e^{-\frac{t}{\tau_B}}\right) \quad (2)$$

We fitted the fluorescence data with Eq. (2) (see continuous lines in Fig. 3), and obtained good agreement between the toy model and the data. The estimated fitting free parameters τ_A and τ_B are similar and their values are about 6.5 ± 0.5 s for all the data. The similarity between the two fitting parameters τ_A and τ_B is unexpected and could be explained considering the following speculative interpretation. The measurements were made on a large population of cells (about 20,000/well). At the single cell level, the Ca–FLUO-4 complex remains fluorescent for a time that is probably similar for each single cell. In the cell population, some cells will be stimulated by TLQP-21 earlier than others, and this explains the kinetic in the measured increase in the fluorescence. On the average, cells should remain fluorescent for a similar time, and this might give rise to similar characteristic in the switch-on and switch-off kinetics. The appropriateness of the proposed simplified model is supported by the quality of the fit, illustrated by the

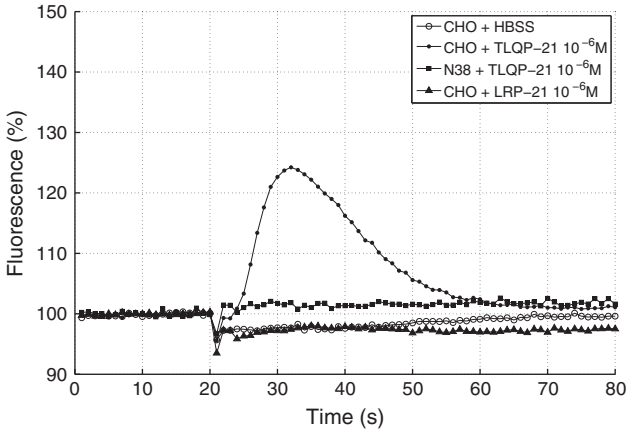

Fig. 2. Control measurements: percentage of the fluorescence (proportional to the free intracellular calcium levels) of the cells after the injection. Effects of the TLQP-21 peptide, of the LRP21 scrambled peptide, of the HBSS on the CHO and N38 cells. See labels for details of peptide concentrations.

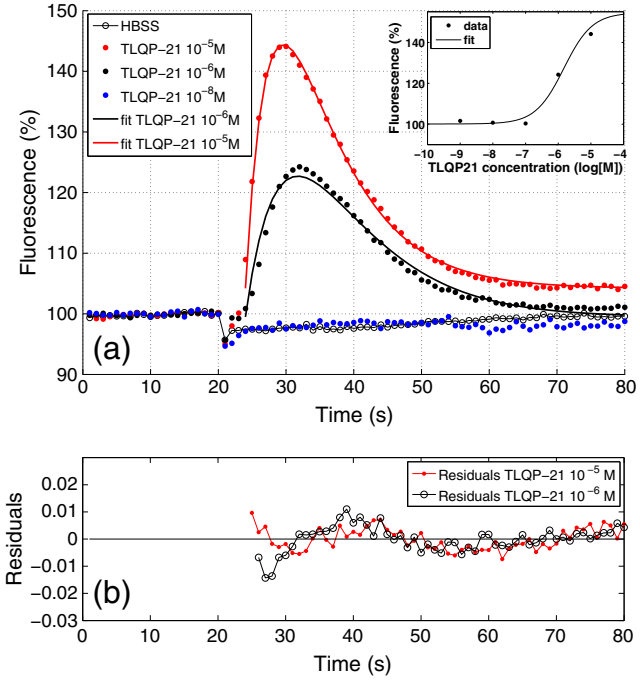

Fig. 3. *Panel a*: measured TLQP-21 stimulation of free intracellular calcium levels in CHO cells (*symbols*) and fit of the data with Eq. (2) (*continuous lines*). TLQP-21 was injected at different concentrations (see labels). *Inset*: Maximal response of TLQP-21 calcium mobilizing activity measured as a function of peptide concentration. *Panel b*: The residuals (i.e. differences between data and the fitting lines shown in the main panel (a)) appear randomly scattered around zero indicating the goodness of the fitting model.

measured coefficients of determination R^2 of 0.9854 and 0.9966 for TLQP-21 at 10^{-5} M and 10^{-6} M, respectively. Furthermore the residuals plotted in Fig. 3(b) appear randomly scattered around zero indicating the goodness of the fitting model despite its very simplified assumptions.

Dose-response studies using CHO demonstrated that TLQP-21 (10^{-9} to 10^{-5}M) induced a concentration-dependent increase in free intracellular calcium levels (Fig. 3). The concentrations of TLQP-21 from 10^{-6} to 10^{-5} M, inclusive, evoked significant increases ($P<0.05$) in intracellular calcium levels (inset of Fig. 3). The dose–response data shown (inset of Fig. 3) represent the maximum value of the attained fluorescence as a function of TLQP-21 concentration and can be described by a Langmuir-like adsorption model, as shown in the following. Considering a standard reversible reaction between a ligand having molarity [L] and a receptor having molarity [R], with a dissociation constant K_d, we have [35,36]:

$$\begin{cases} [L][R] = K_d \cdot [LR] \\ [L_0] = [L] + [LR] \\ [R_0] = [R] + [LR] \end{cases} \quad (3)$$

Where [L] and [R] are the molarity of free ligand and receptor, [LR] is the molarity of ligand-bound receptor, and [L_0] and [R_0] are the initial molarities. Solving the systems of equations we got:

$$[LR] = \frac{1}{2}\left(K_d + [L_0] + [R_0] + + \sqrt{(K_d + [L_0] + [R_0])^2 - 4[L_0][R_0]}\right) \quad (4)$$

Since fluorescence is proportional to the quantity [LR] it is possible to fit the dose–response data (see continuous line of inset of Fig. 3) with the above expression obtaining a value of K_d of the order of 10^{-6}M. Given the uncertainty and the small number of the data it is difficult to have a better estimation of ligand–receptor binding constant, but in any case we obtained a reasonable order of magnitude.

To ascertain the specificity of TLQP-21 effects on calcium release, we used 10^{-6}M LRP-21, a scrambled peptide made using the same aminoacid residues of TLQP-21, and which shares no homology with other known peptides. As shown in Fig. 2, LRP-21 did not stimulate calcium release in CHO cells, confirming the specificity of TLQP-21 effects.

Since we used a biotinilated TLQP-21 (BIO-TLQP-21) bound to the streptavidinated AFM cantilevers, we also checked if the biological activity of this modified peptide was comparable to that of TLQP-21. As shown in Fig. 4, there is a complete overlap of the fluorescence data obtained with biotinilated and standard TLQP-21. Biotinilation of TLQP-21 at the N-terminus did not change its ability to stimulate intracellular calcium release in CHO, thus suggesting that the C-terminal region is primarily involved in the interaction with its binding site.

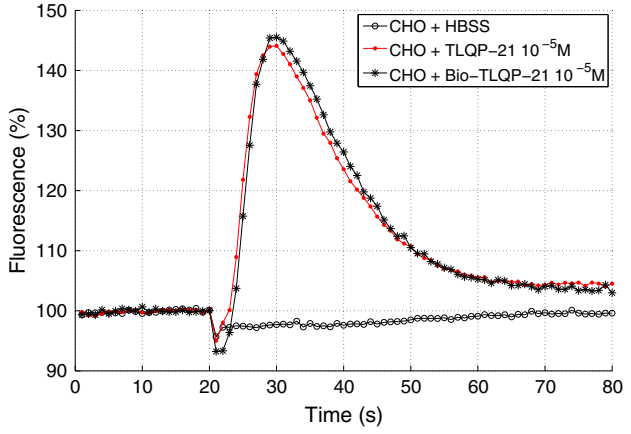

Fig. 4. Comparison between the effects of TLQP-21 and biotin-TLQP-21 on free intracellular calcium in CHO cells. See labels for details.

3.2. Atomic force microscopy

For force measurements, the functionalized tip was located on top of a cell exploiting the capacity of the AFM apparatus to visually inspect the position of the cantilever tip (Fig. 1).

The individual unbinding forces between the TLQP-21 functionalized tip and the cell surface were analyzed from the single force curves extracted from the force map (Fig. 5a and b). Although some retraction curves show no particular features, ~30% of the curves present remarkable pull-off (inset of Fig. 5a). Most likely, the pull-off is due to a binding–unbinding event between TLQP-21 on the tip and its binding sites on the cell membrane. The adhesion force values of all sets were collected and plotted in a force histogram (Fig. 5a). The mean unbinding force between TLQP-21 binding sites and the peptide is 39 ± 7 pN. The single peak of the probability of force distribution suggests the existence of a single class of binding sites. Furthermore, classical binding studies with a radio-labeled analog of TLQP-21 confirm that a single class of binding sites is expressed on CHO cell membranes (data not shown, A. Torsello, to be published).

To verify the specificity of the unbinding events, we performed control experiments on CHO cells with non-functionalized tips and on N38 cells, which do not respond to TLQP-21 (Fig. 2), with both functionalized and non-functionalized tips. We found that the adhesion forces between the functionalized tip and N38 were significantly lower than those on CHO cells (Fig. 5b). These data suggest the

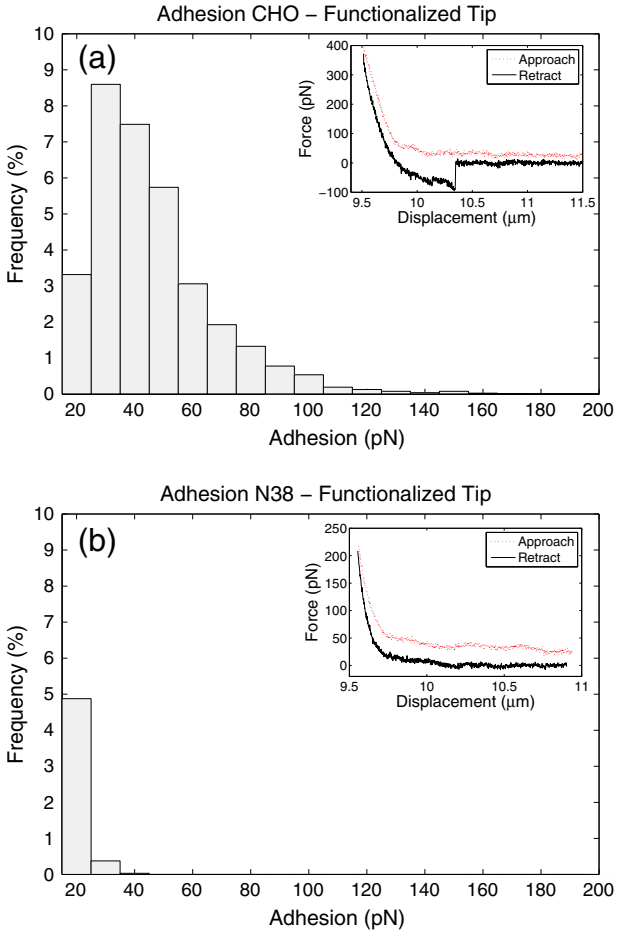

Fig. 5. *Main figures*: Histograms of unbinding forces between TLQP-21 functionalized tip and living cells. Force values were obtained on CHO cells (*Panel a*) and N38 cells (*Panel b*). *Insets*: Representative force plot of AFM measurement obtained on living cell acquired with a functionalized tip. Vertical axis shows the force applied to the cantilever as a function of the cantilever-sample displacement. Typical force curve acquired on CHO cell shows specific unbinding event (i.e. minimum of the curve) (*Inset a*). Force curve on N38 cell shows no particular features (*Inset b*).

absence of TLQP-21 binding sites on N38 cells and imply that the adhesion force measured between CHO cells and TLQP-21-tip should be attributed to the specific interaction of the peptide with its binding site.

The topological distribution of the TLQP-21 binding sites on the cell surface of a representative case is shown in Fig. 6a. This is a 2×2 μm^2 map of the cell surface and the color intensities are proportional to the detachment force between TLQP-21 and the binding site. The brighter dots indicate large force values and consequently the presence of a binding site. Fig. 6a shows a representative case, but we have repeated the force spectroscopy imaging procedure on several cell spots without any significant deviation from the statistical average distributions [37–39]. Since the cell is a tridimensional object, the hypothetical local non-horizontality of the cell surface could potentially cause some bias in the bi-dimensional force scanning. However, the explored areas here reported are relatively small (2×2 μm^2) compared with the actual cell surface. In addition, in order to avoid, or at least to minimize, the morphological contribution, the maps were acquired in the peripheral region, where the cell surface is flatter (see Fig. 1). Moreover, the AFM force spectroscopy measurements of the adhesion forces are sensitive to cantilever detaching and not to its *z* position, so the vertical profile of the cell is not crucial. By visual inspection of Fig. 6a, the binding sites appear randomly distributed, as confirmed by the following derivations. The 2D topological distribution of these binding sites on the surface of the CHO cells can be quantified by evaluating radial distribution function *g(r)* of the representative image data reported in Fig. 6a. Here we assumed that above a threshold value of 10 pN there is a binding site; furthermore, we calculated the coordinates, and we evaluated *g(r)* as the normalized probability of finding a binding site at a distance *r* from another one. First, we calculated the distance distribution between each of the detected binding sites, then we normalized the resulting distribution with the distance distribution of an uniformly scattered ensemble filling completely a square lattice with the same finite dimensions (40×40 pixels^2) [40]. After normalization, the resulting function *g(r)* is plotted in Fig. 6b confirming that the binding sites are on average randomly distributed. As control measurements we have also reported the force spectroscopy maps on three control samples: CHO cells probed by non-functionalized tips (Fig. 6c) and N38 cells probed by both TLQP-21 functionalized and not functionalized tips (Fig. 6d–e). In all these cases the brighter dots were very few and less intense indicating the absence of relevant ligand–receptor interaction.

4. Conclusions

By measuring the fluorescence generated by free intracellular calcium levels and the interaction between TLQP-21 and the cell surface, we were able to demonstrate the presence of specific TLQP-21 binding sites on the surface of CHO cells. These TLQP-21 binding sites interact with the peptide with an average force of 39 ± 7 pN indicating the existence of a single class of binding sites. These findings provide evidence that CHO cells contain significant amounts of TLQP-21 binding sites showing features typical of classical ligand–receptor interaction. Since no receptor has been so-far described for TLQP-21, future research will be devoted to isolate and characterize the binding site expressed by CHO cells and to study its cellular mechanism of action.

Acknowledgements

This research was supported in part by Fondo di Ateneo per la Ricerca of the University of Milano-Bicocca (V.L., A.T., F.M. and D.S.) and FIRB RBNE01JKLF_008 to V.L.

References

[1] A. Bartolomucci, G.L. Corte, R. Possenti, V. Locatelli, A.E. Rigamonti, A. Torsello, E. Bresciani, I. Bulgarelli, R. Rizzi, F. Pavone, F.R. D'Amato, C. Severini, G. Mignogna, A. Giorgi, M.E. Schinina, G. Elia, C. Brancia, G.L. Ferri, R. Conti, B. Ciani, T. Pascucci, G. Dell'Omo, E.E. Muller, A. Levi, A. Moles, TLQP-21, a VGF-derived peptide, increases energy expenditure and prevents the early phase of diet-induced obesity, Proc. Natl. Acad. Sci. U. S. A. 103 (2006) 14584–14589.
[2] E. Trani, A. Giorgi, N. Canu, G. Amadoro, A.M. Rinaldi, P.A. Halban, G.L. Ferri, R. Possenti, M.E. Schinina, A. Levi, Isolation and characterization of VGF peptides in rat brain. role of PC1/3 and PC2 in the maturation of VGF precursor, J. Neurochem. 81 (2002) 565–574.
[3] A.N. van den Pol, K. Bina, C. Decavel, P. Ghosh, VGF expression in the brain, J. Comp. Neurol. 347 (1994) 455–469.

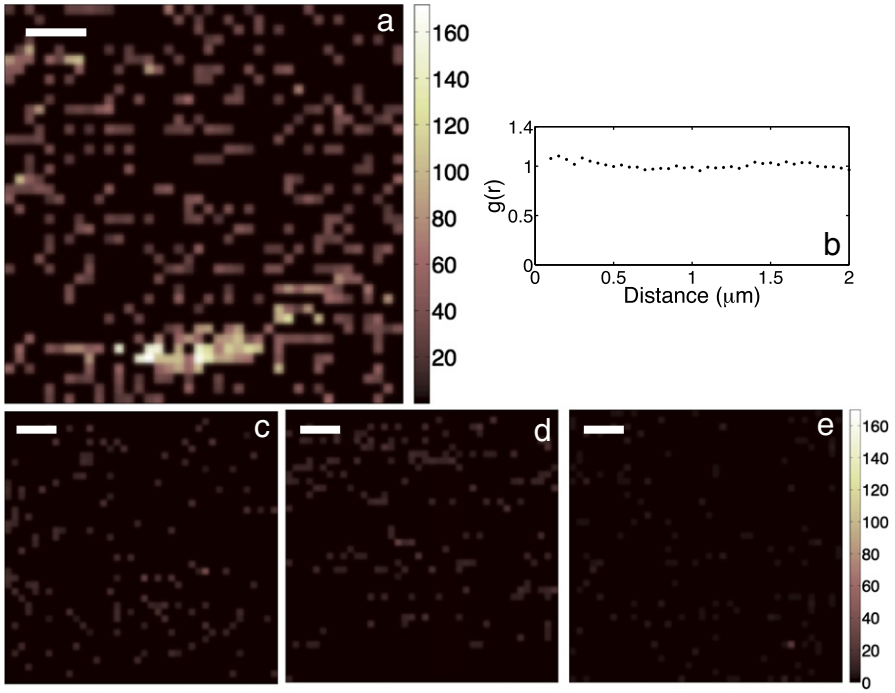

Fig. 6. Panel (a), (c)–(e): Representative two dimensional adhesion maps (2×2 μm^2, scale bars: 300 nm) of the receptor distribution on a cell surface obtained with: (a) a cantilever functionalized with TLQP-21 on CHO cell; (c) a non-functionalized tip on CHO cell; (d) a functionalized tip on N38 cell; (e) a non-functionalized tip on N38 cell. The color scale on the right shows the force strength of the adhesion in pN. Panel b: radial distribution function g(r) of the representative image data shown in panel (a).

[4] S.R. Salton, G.L. Ferri, S. Hahm, S.E. Snyder, A.J. Wilson, R. Possenti, A. Levi, VGF: a novel role for this neuronal and neuroendocrine polypeptide in the regulation of energy balance, Front. Neuroendocrinol. 21 (2000) 199–219.
[5] A. Levi, G.L. Ferri, E. Watson, R. Possenti, S.R. Salton, Processing, distribution, and function of VGF, a neuronal and endocrine peptide precursor, Cell. Mol. Neurobiol. 24 (2004) 517–533.
[6] C. Severini, G.L. Corte, G. Improta, M. Broccardo, S. Agostini, C. Petrella, V. Sibilia, F. Pagani, F. Guidobono, I. Bulgarelli, G.L. Ferri, C. Brancia, A.M. Rinaldi, A. Levi, R. Possenti, In vitro and in vivo pharmacological role of TLQP-21, a VGF-derived peptide, in the regulation of rat gastric motor functions, Br. J. Pharmacol. 157 (2009) 984–993.
[7] E. Trani, T. Ciotti, A.M. Rinaldi, N. Canu, G.L. Ferri, A. Levi, R. Possenti, Tissue-specific processing of the neuroendocrine protein VGF, J. Neurochem. 65 (1995) 2441–2449.
[8] C. Brancia, C. Cocco, F. D'Amato, B. Noli, F. Sanna, R. Possenti, A. Argiolas, G.L. Ferri, Selective expression of TLQP-21 and other VGF peptides in gastric neuroendocrine cells and modulation by feeding, J. Endocrinol. 207 (2010) 329–341.
[9] F. D'Amato, B. Noli, C. Brancia, C. Cocco, G. Flore, M. Collu, P. Nicolussi, G.L. Ferri, Differential distribution of VGF-derived peptides in the adrenal medulla and evidence for their selective modulation, J. Endocrinol. 197 (2008) 359–369.
[10] S. Hahm, T.M. Mizuno, T.J. Wu, J.P. Wisor, C.A. Priesta, C.A. Kozak, C.N. Boozer, B. Peng, R.C. McEvoy, P. Good, K.A. Kelley, J.S. Takahashi, J.E. Pintar, J.L. Roberts, C.V. Mobbs, S.R. Salton, Targeted deletion of the VGF gene indicates that the encoded secretory peptide precursor plays a novel role in the regulation of energy balance, Neuron 23 (1999) 537–548.
[11] S. Hahm, C. Fekete, T.M. Mizuno, J. Windsor, H. Yan, C.N. Boozer, C. Lee, J.K. Elmquist, R.M. Lechan, C.V. Mobbs, S.R. Salton, VGF is required for obesity induced by diet, gold thioglucose treatment, and agouti and is differentially regulated in pro-opiomelanocortin and neuropeptide Y-containing arcuate neurons in response to fasting, J. Neurosci. 22 (2002) 6929–6938.
[12] P.H. Jethwa, A. Warner, K.N. Nilaweera, J.M. Brameld, J.K. Keyte, W.G. Carter, N. Bolton, M. Bruggraber, P.J. Morgan, P. Barrett, F.J. Ebling, VGF-derived peptide, TLQP-21, regulates food intake and body weight in siberian hamsters, Endocrinology 148 (2007) 4044–4055.
[13] R. Rizzi, A. Bartolomucci, A. Moles, F. D'Amato, P. Sacerdote, A. Levi, G.L. Corte, M.T. Ciotti, R. Possenti, F. Pavone, The VGF-derived peptide TLQP-21: a new modulatory peptide for inflammatory pain, Neurosci. Lett. 441 (2008) 129–133.
[14] A. Bartolomucci, A. Moles, A. Levi, R. Possenti, Pathophysiological role of TLQP-21: gastrointestinal and metabolic functions, Eat. Weight. Disord. 13 (2008) e49–e54.
[15] V. Sibilia, F. Pagani, I. Bulgarelli, G. Tulipano, R. Possenti, F. Guidobono, Characterization of the mechanisms involved in the gastric antisecretory effect of TLQP-21, a VGF-derived peptide, in rats, Amino Acids 42 (2012) 1261–1268.
[16] R. Possenti, G. Muccioli, P. Petrocchi, C. Cero, A. Cabassi, L. Vulchanova, M.S. Riedl, M. Manieri, A. Frontini, A. Giordano, S. Cinti, P. Govoni, G. Graiani, F. Quaini, C. Ghè, E. Bresciani, I. Bulgarelli, A. Torsello, V. Locatelli, V. Sanghez, B.D. Larsen, J.S. Petersen, P. Palanza, S. Parmigiani, A. Moles, A. Levi, A. Bartolomucci, Characterization of a novel peripheral pro-lipolytic mechanism in mice: role of VGF-derived peptide TLQP-21, Biochem. J. 441 (2012) 511–522.
[17] V. Cassina, D. Seruggia, G.L. Beretta, D. Salerno, D. Brogioli, S. Manzini, F. Zunino, F. Mantegazza, Atomic force microscopy study of DNA conformation in the presence of drugs, Eur. Biophys. J. 40 (2011) 59–68.
[18] M. Gregori, V. Cassina, D. Brogioli, D. Salerno, L.D. Kimpe, W. Scheper, M. Masserini, F. Mantegazza, Stability of A beta (1-42) peptide fibrils as consequence of environmental modifications, Eur. Biophys. J. 39 (2010) 1613–1623.
[19] S. Allen, X. Chen, J. Davies, M.C. Davies, A.C. Dawkes, J.C. Edwards, C.J. Roberts, J. Sefton, S.J.B. Tendler, P.M. Williams, Detection of antigen–antibody binding events with the atomic force microscope, Biochemistry 36 (1997) 7457–7463.
[20] H. Kim, H. Arakawa, T. Osada, A. Ikai, Quantification of cell adhesion force with AFM: distribution of vitronectin receptors on a living MC3T3-E1 cell, Ultramicroscopy 97 (2003) 359–363.
[21] H. Kim, H. Arakawa, N. Hatae, Y. Sugimoto, O. Matsumoto, T. Osada, A. Ichikawa, A. Ikai, Quantification of the number of EP3 receptors on a living CHO cell surface by the AFM, Ultramicroscopy 106 (2006) 652–662.
[22] P. Hinterdorfer, Y.F. Dufrene, Detection and localization of single molecular recognition events using atomic force microscopy, Nat. Methods 3 (2006) 347–355.
[23] E.L. Florin, V.T. Moy, H.E. Gaub, Adhesion forces between individual ligand–receptor pairs, Science 264 (1994) 415–417.
[24] P. Hinterdorfer, W. Baumgartner, H.J. Gruber, K. Schilcher, H. Schindler, Detection and localization of individual antibody–antigen recognition events by atomic force microscopy, Proc. Natl. Acad. Sci. U. S. A. 93 (1996) 3477–3481.
[25] V. Dupres, C. Verbelen, D. Raze, F. Lafont, Y.F. Dufrene, Force spectroscopy of the interaction between mycobacterial adhesins and heparan sulphate proteoglycan receptors, ChemPhysChem 10 (2009) 1672–1675.
[26] E.P. Wojcikiewicz, X. Zhang, V.T. Moy, Force and compliance measurements on living cells using atomic force microscopy (AFM), Biol. Proced. Online 6 (2004) 1–9.
[27] V.T. Moy, E.L. Florin, H.E. Gaub, Adhesive forces between ligand and receptor measured by AFM, Colloids Surf. 93 (1994) 343–348.
[28] D. Salerno, D. Brogioli, V. Cassina, D. Turchi, G.L. Beretta, D. Seruggia, R. Ziano, F. Zunino, F. Mantegazza, Magnetic tweezers measurements of the nanomechanical properties of DNA in the presence of drugs, Nucleic Acids Res. 38 (2010) 7089–7099.
[29] D. Salerno, A. Tempestini, I. Mai, D. Brogioli, R. Ziano, V. Cassina, F. Mantegazza, Single-molecule study of the DNA denaturation phase transition in the force-torsion space, Phys. Rev. Lett. 109 (2012) 118303.
[30] D.H. Paik, T.T. Perkins, Overstretching DNA at 65 pn does not require peeling from free ends or nicks, J. Am. Chem. Soc. 133 (2011) 3219–3221.
[31] J. Wong, A. Chilkoti, V.T. Moy, Direct force measurements of the streptavidin–biotin interaction, Biomol. Eng. 16 (1999) 45–55.
[32] D. Alsteens, M.C. Garcia, P.N. Lipke, Y.F. Dufrene, Force-induced formation and propagation of adhesion nanodomains in living fungal cells, Proc. Natl. Acad. Sci. U. S. A. 107 (2010) 20744–20749.
[33] A. Yersin, T. Osada, A. Ikai, Exploring transferrin–receptor interactions at the single-molecule level, Biophys. J. 94 (2008) 230–240.
[34] V. Montana, W. Liu, U. Mohideen, V. Parpura, Single molecule measurements of mechanical interactions within ternary SNARE complexes and dynamics of their disassembly: SNAP25 vs. SNAP23, J. Physiol. 587 (9) (2009) 1943–1960.
[35] T. Bellini, V. Degiorgio, F. Mantegazza, F.A. Marsan, C. Scarnecchia, Electrokinetic properties of colloids of variable charge. I. Electrophoretic and electro-optic characterization, J. Chem. Phys. 103 (1995) 8228.
[36] D.J. Bornhop, J.C. Latham, A. Kussrow, D.A. Markov, R.D. Jones, H.S. Sorensen, Free-solution, label-free molecular interactions studied by back-scattering interferometry, Science 317 (2007) 1732–1736.
[37] E. Spedden, J.D. White, E.N. Naumova, D.L. Kaplan, C. Staii, Elasticity maps of living neurons measured by combined fluorescence and Atomic Force Microscopy, Biophys. J. 103 (2012) 868–877.
[38] M. Hu, J. Chen, J. Wang, X. Wang, S. Ma, J. Cai, C.Y. Chen, Z.W. Chen, AFM- and NSOM-based force spectroscopy and distribution analysis of CD69 molecules on human CD4+ T cell membrane, J. Mol. Recognit. 22 (2009) 516–520.
[39] P. Hinterdorfer, M.F. Garcia-Parajo, Y.F. Dufrene, Single-molecule imaging of cell surfaces using near-field nanoscopy, Acc. Chem. Res. 45 (2012) 327–336.
[40] M.M. Baksh, M. Jaros, J.T. Groves, Detection of molecular interactions at membrane surfaces through colloid phase transitions, Nature 427 (2004) 139–141.